RSC Advances

PAPER

View Article Online
View Journal | View Issue

Cite this: *RSC Adv.*, 2017, **7**, 39443

Zinc dopant inspired enhancement of electron injection for $CuInS_2$ quantum dot-sensitized solar cells†

Qinqin Wu,[a] Chunqi Cai,[a] Lanlan Zhai,[a] Jiantao Wang,[a] Fantai Kong,[b] Yun Yang,[a] Lijie Zhang,[a] Chao Zou*[a] and Shaoming Huang*[a]

Received 14th June 2017
Accepted 4th August 2017

DOI: 10.1039/c7ra06659g

rsc.li/rsc-advances

After being doped with zinc, $CuInS_2$ quantum dots (QDs) exhibit desired tunable optical and electronic properties, more specifically, photoluminescence emission and band gap. The former is mainly due to the intrinsic donor–acceptor transition, which, together with the improved quantum yield and large longest decay time, accounts for 95% of the whole emission profiles. The latter results in an enhanced k_{et} value of 2.99×10^{10} s^{-1}, greater than that for pure $CuInS_2$ QDs by an order of magnitude. Functioning as light harvesting materials in quantum dot sensitized solar cells, zinc doped $CuInS_2$ QDs show broadened photoresponse up to ~950 nm. Incident photon-to-current conversion efficiency of quantum dot sensitized solar cells achieves a maximum of 69% at 500 nm and can be maintained over 50% within the window below 750 nm. After the doping with zinc under optimized conditions, the average power conversion efficiency of solar cells under one full sun illumination demonstrates an increase of 13.2%, from 5.21% for pure $CuInS_2$ QDs to 5.90% for doped $CuInS_2$ QDs. It is proven that the improved performance can be attributed to a broadened optoelectronic response range and accelerated electron injection.

1. Introduction

Due to quantum confinement and enhanced surface to volume ratios, colloidal quantum dots (QDs) provide a unique platform for designing new applications in solar cells, LEDs, and photocatalysts.[1] The flexibility of QDs may lead to controllable band edge energies and composition, tunable bandgap onset energies, strong optical transitions, facile doping and synthesis strategies, and enhanced multiple exciton generation (MEG).[2–6] Recently, quantum dot-sensitized solar cells (QDSCs) have drawn great attention with the use of QDs for the development of a suitable sensitizer in the next generation of photovoltaic technologies.[7,8] Power Conversion Efficiencies (PCE) up to 11.16% and 11.61% based on CdSeTe and Zn–Cu–In–Se QDSCs, respectively, were reported by Zhong and coworkers.[9,10] Functioning as sensitizers, QDs play vital roles in terms of light harvesting and corresponding electron injection.[11–13] The recent emergence of ternary I–III–VI_2 QDs offers a promising alternative to the binary chalcogenide QDs for their enhanced tunable optical and electronic properties, in addition to ecofriendliness.[14,15]

As a typical I–III–VI_2 semiconductor,[16] $CuInS_2$ possessing direct band gap displays high absorbing coefficient and good stability under solar radiation, and is compatible with the AM0 solar spectrum ($E_g = 1.5$ eV).[17–19] These properties make $CuInS_2$ QDs a good candidate as the sensitizer in quantum dot-sensitized solar cells.[8] In order to meet the increasingly demand of effective solar cells, considerable efforts have been made to improve the performance of $CuInS_2$ QDs based QDSCs.[8,18,20–23] Zhong and Hyeon groups have reported high performance QDSCs with PCE of 7.04% (ref. 23) for $CuInS_2$/ZnS and 8.10% for $CuInSe_2$,[24] respectively. However, the potential of QDSCs has yet to be fully demonstrated. Beneficial from MEG, the theoretical PCE of QDSCs could reach up to 44%.[2,25]

To further boost the efficiency of QDSCs, it is desired to obtain suitable QDs, which are featured by wide absorption range, high conduction band edge, and limited trap state defects, using simple and reproducible processes.[26,27] It has been demonstrated that type-I core/shell structured QDs developed by the overgrowth of wider band gap ZnS or CdS shell on QDs have enhanced luminescent emission efficiency and stability.[28] For example, Zhong and coworkers showed type-I core/shell QDs based QDSCs with PCE over 9% for CdSeTe/CdS[29] and 7.04% for $CuInS_2$/ZnS,[23] respectively. However, the overgrowth of shell on QDs core may reduce charge recombination and act as injection barrier, which have conflicting

[a]Zhejiang Key Laboratory of Carbon Materials, College of Chemistry and Material Engineering, Wenzhou University, Wenzhou 325027, Zhejiang, People's Republic of China. E-mail: zouchao@wzu.edu.cn; smhuang@wzu.edu.cn

[b]Key Laboratory of Novel Thin Film Solar Cells, Hefei Institute of Physics Science, Chinese Academy of Sciences, Hefei 230088, Anhui, People's Republic of China

† Electronic supplementary information (ESI) available: Quantum yields of ZCIS QDs, photovoltaic parameters of corresponding QDSCs. See DOI: 10.1039/c7ra06659g

effects on effective electron transportation.[23] It is difficult to make a compromise between these two effects. In addition, the conventional syntheses by two separated steps for core and shell growths using Schlenk technology are neither easy nor reproducible, even after decades from the appearance of colloidal method.[28,30] Doped QDs provide a promising alternative.[31] Dopant could alter electron wave in orbitals of host QDs, producing moderate modulation on band gaps and further on conduction band edges,[30,32] hence, promoting electron injection from QDs to TiO_2 photoanodes. Additionally, ternary $CuInS_2$ QDs tolerate a large range of off-stoichiometric compositions and complex crystal structure relevant with donor and acceptor trap states.[15,33–36] Donor and acceptor sub-bandgap states are originated from Cu and In vacancies (V_{Cu} and V_{In}) and replacing defects (Cu_{In} and In_{Cu}).[35–37] It has been shown that donor and acceptor trap states in QDs could be adapted by the incorporation of dopant into the host structure. The successes of Zn–Cu–In–Se,[10] Cu–In–Ga–Se,[38] $CuInSe_xS_{2-x}$ (ref. 18) and Zn–Ag–In–Se[39] QDs have been validated. Noted is that both of the two reports on QDSCs with PCE above 11% were conducted under the assistant of highly catalytic Ti/C counter electrodes rather than on conventional Cu_2S/brass.

Herein, a facile synthesis of zinc doped $CuInS_2$ QDs with tunable photoluminescence is presented. A series of zinc doped $CuInS_2$ QDs that is capped by oleylamine were synthesized by thermal decomposition of organometallic precursors. It was shown that tunable photoluminescence (PL), long lifetime and enhanced quantum yield (QY) of zinc doped $CuInS_2$ QDs are mainly attributed to the donor–acceptor pair recombination, which accounts for over 95% of the whole emission profiles. Water-soluble zinc doped $CuInS_2$ QDs were tethered on mesoporous TiO_2 film electrode after ligand exchange. The fabricated zinc doped $CuInS_2$ QDs-based QDSCs exhibit photoresponse extended to ~950 nm and achieve average PCE of 5.90% under one full sun illumination.

2. Experimental

2.1 Materials

All chemicals were used as received without further purification. Copper diethyldithiocarbamate ($Cu(dedc)_2$, 97.0%) and zinc diethyldithiocarbamate ($Zn(dedc)_2$, 99%) were obtained from TCI; indium nitrate ($In(NO_3)_3$, 99.9%) from Alfa Aesar; sodium diethyldithiocarbamate trihydrate (Na(dedc), 99%), and *n*-hexane (95%) from J&K; oleylamine (>80%), dodecanethiol (98%), and mercaptopropionic acid (MPA, >99%) from Acros.

2.2 Synthesis of $In(dedc)_3$ precursors

The $In(dedc)_3$ precursors were synthesized according to the previous reports.[40] In a typical synthesis of $In(dedc)_3$, Na(dedc) (6 mmol) and $In(NO_3)_3$ (2 mmol) were respectively dissolved in 100 mL and 50 mL de-ionized water, then the $In(NO_3)_3$ solution was added dropwise to the Na(dedc) solution with magnetic stirring. The white product was washed 3 times with de-ionized water and dried under a vacuum at 60 °C for 3 h. As-synthesized precursors were stored in desiccator at room temperature.

2.3 Synthesis of zinc doped $CuInS_2$ QDs with tunable composition

Zinc doped $CuInS_2$ QDs with tunable compositions can be achieved by varying the relative molar ratio of precursors in the source materials. In a typical synthesis of zinc doped $CuInS_2$ QDs (ZCIS-10), $Cu(dedc)_2$ (0.05 mmol), $In(dedc)_3$ (0.1 mmol) and $Zn(dedc)_2$ (0.01 mmol) were loaded into a 50 mL rounded-bottom flask, which was then filled with 4 mL of oleylamine. After ultrasonic dispersing at room temperature, magnetic stirring at room temperature was followed. The flask was immersed into oil bath and maintained at 180 °C for 20 min and then allowed to cool to room temperature by water bath. The red dark product was collected by centrifugation, washed several times with absolute ethanol and *n*-hexane. Pure $CuInS_2$ QDs were synthesized with the absence of zinc precursors. For simplicity, the sample for zinc doped $CuInS_2$ QDs with the ratio of Zn/In precursors 0.025 was referred ZCIS-2.5 and so on.

2.4 Ligand exchange of QD and fabrication of TiO_2 photoanodes

Ligand exchange of oil-soluble ZCIS QD to water-soluble QDs was performed according to a literature method. Typically, 0.4 mmol MPA was first dissolved in 1.0 mL methanol, then the pH of the solution was adjusted to 11 with the use of 30% NaOH aqueous solution. The MPA solution was added into 15 mL ZCIS QDs dichloromethane solution and stirred for 30 min to get the precipitation of the ZCIS QDs. Then 10.0 mL de-ionized water was added into the mixture and kept the stirring for another 20 min. The solution was separated into two phases and the ZCIS QDs were transferred into the superincumbent water from the underlying chloroform, the underlying phase was discarded and the aqueous phase containing the MPA-capped ZCIS QDs was collected. The aqueous dispersion was further purified by centrifugation and decantation with the addition of acetone, and the precipitate was redissolved in 1.0 mL de-ionized water.

The double layered mesoporous TiO_2 photoanodes were fabricated on well-cleaned FTO glass. Before the 10.0 μm thick transparent 20 nm-TiO_2 layer was coated on the FTO substrate by successive screen-printing of TiO_2 paste, the cleaned FTO glass was treated with 40 mM $TiCl_4$ aqueous solution for the formation of a compact TiO_2 layer on substrate, followed by another screen-printing of 2.0 μm thick light scattering 200 nm-TiO_2 layer. Finally, the film was heat treated in a hot plate at 500 °C for 30 min.

The doped $CuInS_2$ QD sensitizers were immobilized on the TiO_2 mesoporous films by pipetting 30 μL QD aqueous dispersion (absorbance of 3.0 and pH of 11.0) onto the film surface and maintaining 4 h before rinsed sequentially with de-ionized water and ethanol and then dried with nitrogen. After the immobilization, the sensitized TiO_2 films were coated with ZnS, alternately dipping into 0.1 M $Zn(NO_3)_2$ and 0.1 M Na_2S solution for 1 min, rinsing with ethanol between dips.

2.5 Assembling solar cells

The sandwich-type cells were constructed by assembling the photoanode and the Cu_2S/brass counter electrode using

a 50 μm thick Scotch spacer. To prepare Cu_2S/brass counter electrode, brass foil was immersed in HCl solution (1.0 M) at 80 °C for 15 min and subsequently soaked into polysulfide electrode solution for 2 min. The polysulfide electrode solution was obtained by the dissolution of 2.0 M Na_2S, 2.0 M S, and 0.2 M KCl in de-ionized water. A droplet (10 μL) of polysulfide electrolyte was injected into the cell device. The area of the cells was 0.25 cm^2. For QDSCs fabricated under each condition, several cells were performed and tested in parallel.

2.6 Characterization

The as-synthesized sample were drop cast on the Si low background sample holders and dried at room temperature in the air, then the powder X-ray diffraction (XRD) patterns of the prepared samples were recorded on Bruker D8 advance X-ray diffractometer with graphite monochromatized Cu Kα (λ = 1.5405 Å) radiation with a step of 0.02° at a scanning speed of 4° min^{-1} in 2θ ranging from 10° to 80°. Scanning electron microscopy (SEM) images were taken using a FEI Nova Nano-SEM200 microscope. Composition analysis was performed by EDS (oxford INCA). The transmission electron microscopy (TEM) was carried out under JEOL JEM-2100F microscope operating at an accelerating voltage of 200 kV. UV-visible (UV-vis) absorption spectra of the samples were recorded on a SHIMADZU UV-1800 spectrophotometer. Steady-state photoluminescence (PL) spectra and absolute quantum yield (QY) were measured using a Fluoromax-4 spectrofluorometer (HORIBA Jobin Yvon Inc.) equipped with a 150 W xenon lamp as the excitation source. The absolute QYs of the samples were determined by measuring emission and scattered light from the sample and reference in an integrating sphere.[41,42] All the samples were dispersed in dichloromethane and placed in a cuvette inside the integrating sphere. The emitted and scatted radiation was collected at 90° angle from the excitation, and a baffle was placed beside the sample on the emission monochromator side to avoid the collection of directly scatted light. The PL decay dynamics were measured using time-correlated single photon counting (TCSPC) set-up from Jobin Yvon equipped with a 454 nm LED excitation source. Photocurrent density–photovoltage curves (*J*–*V*) of QDSCs were derived with a Keithley 2400 digital source meter (Keithley, USA) under AM 1.5G illumination (100 mW cm^{-2}) by Oriel Sol 3A Solar Simulator (94023A, Newport Stratford Inc., USA), calibrated with a standard crystalline silicon solar cell. The incident photon-to-current conversion efficiency (IPCE) was measured by using solar cell quantum efficiency measurement system (QEX10, PV Measurements, Inc.), and was calibrated with a NREL-certified Si diode before measurement.

3. Results and discussion

Ternary $CuInS_2$ QDs tolerate a large range of off-stoichiometric compositions and complex crystal structures relevant with donor and acceptor trap states, which have significant effects on their optical and electronic properties.[16] Doping zinc ionic into QDs could disturb electron waves in orbits and enhance electronic coupling, hence, also affecting the optoelectronic properties of host $CuInS_2$ QDs. The absorbance spectra of zinc doped $CuInS_2$ QDs with different zinc contents are shown in Fig. 1. While they don't exhibit obvious exciton absorption peaks, the doped QDs apparently have a series of absorbance edges ranging from *ca.* 800 nm to *ca.* 670 nm. A substantial blue shift of the optical absorbance band edges occurs with increased concentration of doped zinc in $CuInS_2$ QDs, indicating an increase in the determined optical band gaps of the doped QDs. The optical band gaps of doped QDs can be derived in the range of 1.55–1.85 eV. High-resolution TEM images (Fig. 2a and b) show that the doped $CuInS_2$ QDs have uniform diameters around 5 nm, independent of zinc concentration, suggesting minor quantum confinement effects. Therefore, the observed blue shift is mainly attributed to the widening of band gaps as a result of the doped zinc. Quantitative elemental analyses of the QDs by EDS (Table 1) suggested the compositions of the QDs were roughly but systemically consistent with the fed Cu/In molar ratios.

TEM image also shows that an individual QD has a clear lattice fringe with interplanar spacing of 3.1 Å, which can be resolved as (112) lattice fringes and agrees well with those determined from diffraction peak at 27.88° in the XRD patterns, demonstrating crystalline nature of doped $CuInS_2$ QDs. Furthermore, XRD patterns (Fig. 2c) exhibit three broad peaks at 2θ = 27.88°, 47.28°, and 55.06°, which are assigned to the diffractions of the (112), (204), and (312) planes of the chalcopyrite $CuInS_2$ crystals, respectively. The three main peaks in XRD pattern shows wider full-width at half-maximum (FWHM) than bulk $CuInS_2$, which can be explained by the broadening effect of nanometer size of QDs. XRD analysis demonstrates that zinc doped $CuInS_2$ QDs with different contents have a chalcopyrite phase. With increased doped zinc concentration, the major diffraction peaks essentially keep stable and no

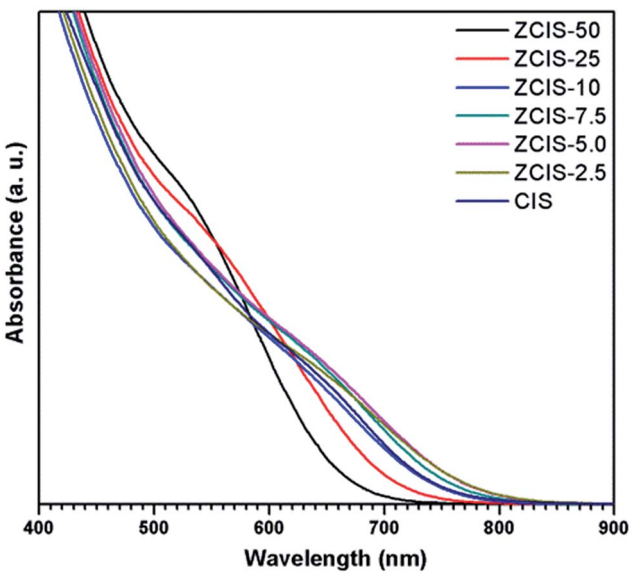

Fig. 1 UV-vis spectra of zinc doped $CuInS_2$ QDs with different contents.

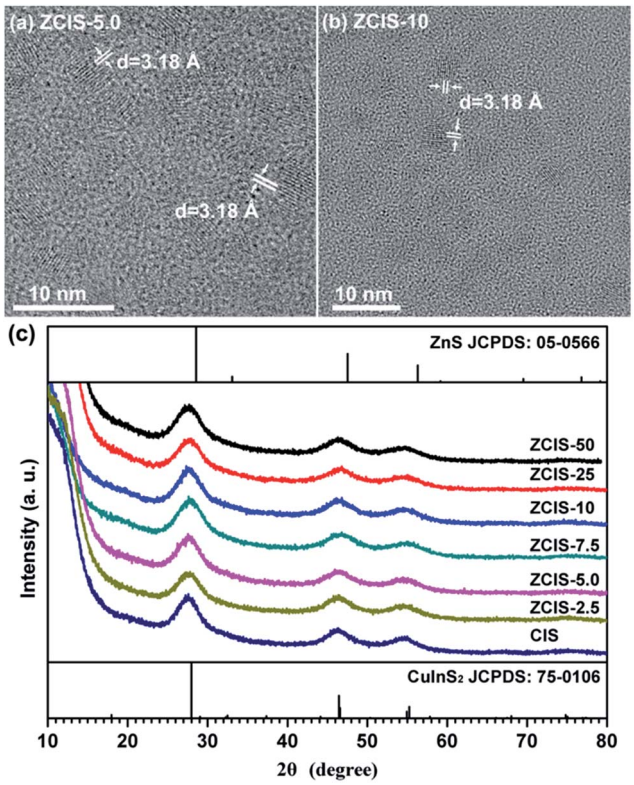

Fig. 2 (a, b) Typical TEM image of doped $CuInS_2$ QDs, and (c) XRD patterns of doped $CuInS_2$ QDs with different zinc contents.

splitting appears. This indicates the incorporation of zinc ions into $CuInS_2$ crystals and rules out phase separation or individual nucleation of ZnS during the synthesis. It may therefore be concluded that the doped zinc is homogeneous distributed in $CuInS_2$ QDs matrix.

PL spectra of zinc doped $CuInS_2$ QDs (Fig. 3a) display broad blue shift emission peaks with higher zinc contents, from 760 nm for ZCIS-2.5 to 680 nm for ZCIS-50. It should be noted that the blue shifted PL peaks for ZnS shell was within a smaller degree than that for zinc alloying QDs. By introducing zinc ions, ZnS–$CuInS_2$ alloy compounds would be formed *via* alloying ZnS with a wider band gap and $CuInS_2$ with a narrower band gap. The band gap of doped $CuInS_2$ QDs becomes wider with the increased contents of doped zinc. The PL peaks of doped $CuInS_2$ QDs exhibit large FWHM from 137 nm for ZCIS-2.5 to 104 nm for ZCIS-50. Usually, large FWHM is observed in the ternary I–III–VI semiconductor QDs due to the characteristic donor–acceptor pair transition or surface defect states.[8,34]

The sensitivity of QY with zinc concentration was investigated (Fig. S1†). The results showed that a minor content of zinc (ZCIS-2.5) may increase QY from 0.2% for pure $CuInS_2$ QDs to 1.9%, approximately by a magnitude order. QY keeps increasing with increased zinc content to 3.1% for ZCIS-5.0, and 4.7% for ZCIS-7.5, 4.2% for ZCIS-10, 4.2% for ZCIS-25, and 4.9% for ZCIS-50. The low QY of pure $CuInS_2$ QDs indicates the extensive existence of surface defect and/or internal trap state, the latter of which can be effectively suppressed by the doping of zinc. It has been reported that QY can also be increased by overcoating wider band gap ZnS or CdS layer on $CuInS_2$ QDs. Klimov *et al.* demonstrated QY of $CuInS_2$ nanocrystals could reach as high as 80% after CdS overcoating growth.[28] Zhong and coworkers reported $CuInS_2$/ZnS core/shell structured QDs with QY 10-fold higher than that of $CuInS_2$ QDs.[23] Many studies have reported QY of ternary nanocrystals with widely ranged values,[17,43–45] which are affected by several factors such as synthesis strategy, types of ligands, cation ratios, and core/shell structure. Deng *et al.*[44] reported Cu–Zn–In–S nanocrystals with QY as high as over 70–80%. According to those strategies on synthesis, dodecanethiol was used as capping agent. Most studies on semiconductor nanocrystals used dodecanethiol and oleylamine, which controls the reactivity of metal ions by tailoring the phase and shape of targets.[15,17,28,30,40,44] However, dodecanethiol would hinder electron transport for tight adsorbance on QD surface in photovoltaic application,[23,46] and thus was avoided in the present work on purpose.

The intrinsic defects, surface defects, and size-dependent band gap of QDs are involved in the PL emission.[34] Different electron–hole recombination mechanisms may correspond to different PL decay lifetimes. To understand the mechanisms underlying the dependence of QY on zinc contents, PL decay dynamics of doped $CuInS_2$ QDs were investigated by time correlated single photon counting (TCSPC) technique. As shown in Fig. 3b, their PL decay curves can be fitted by biexponential equation $I(t) = \alpha_1 \exp(-t/\tau_1) + \alpha_2 \exp(-t/\tau_2)$.[47] Also, the average lifetimes τ_{ave} is used to estimate the PL decay time, which can be defined by $\tau_{ave} = (\alpha_1\tau_1^2 + \alpha_2\tau_2^2)/(\alpha_1\tau_1 + \alpha_2\tau_2)$. The fractional intensities F_1, defined as $(\alpha_1\tau_1)/(\alpha_1\tau_1 + \alpha_2\tau_2)$, gives the weights of the two components and signifies the proportion of the excited state population that radiatively decays through each pathway.

Table 1 The elemental analyses of zinc-doped $CuInS_2$ QDs with gradient composition (EDS)

QDs	Cu (atom%)	In (atom%)	S (atom%)	Zn (atom%)	Zn/In ratios in QDs (%)
ZCIS-50	21.41	18.64	56.33	3.63	19.5
ZCIS-25	23.67	20.65	53.46	2.22	10.8
ZCIS-10	22.42	22.94	53.53	1.11	4.8
ZCIS-7.5	24.05	22.08	52.72	1.15	5.2
ZCIS-5.0	23.23	21.28	54.71	0.79	3.7
ZCIS-2.5	24.38	22.50	52.53	0.60	2.7
CIS	22.53	22.02	55.46	—	—

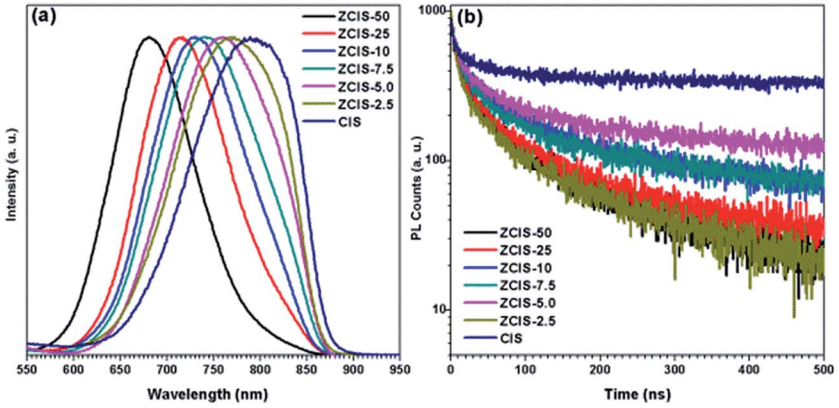

Fig. 3 PL emission spectra (a) and decay curves (b) of doped $CuInS_2$ QDs with different contents.

As shown in Table 2, the PL relaxations can be decomposed into fast and slow decay components. The fast decay components are within tens of nanoseconds with contributions of less than 5%, while the slow decay parts are hundreds of nanoseconds and account for more than 95% to the whole emission profiles. With increased zinc content, the lifetimes of fast components keep stable with enlarged shares, while the lifetimes of slow components decrease with reduced shares. The fast decay (19–25 ns, depending on doped zinc contents) can be attributed to the intrinsic recombination of core states and surface defect states. The slow decay (160–180 ns) is due to donor–acceptor pair transition, which can be verified by the aforementioned broad emission peaks of the doped $CuInS_2$ QDs (FWHM of the peaks is distributed within range of 104–137 nm). It is well known that intrinsic defects in ternary $CuInS_2$ semiconductors are deep trap states for their enhanced configurable degree of freedom in atomic packing models.[34,48] Zhang *et al.*[45] also reported similar results that, in ZnS–$CuInS_2$ alloyed nanocrystals, donor–acceptor transition accounts for a large fraction of the total PL emission spectra. Castro *et al.*[49] attributed some donor and acceptor states for the origin of fluorescence of $CuInS_2$ QDs to sulfur vacancy and copper indium substitution as the donor, cupper vacancy as the acceptor. Sulfur vacancy and interstitial copper create donor levels, and copper vacancy and interstitial sulfur act as acceptor levels in $CuInS_2$ QDs.[50–52] Therefore, cation vacancy plays a fundamental role in donor–acceptor pair mechanism of PL.

During water-soluble ligand exchange in base circumstance, the reactivity of the MPA was enhanced by removing the thiolic hydrogen with a strong base, which ensured a dense and compact coverage of the MPA ligand on the surface of QDs by the thiolic end.[53] MPA-capped doped $CuInS_2$ QDs were deposited and absorbed onto the surface of TiO_2 mesoporous films, facilitated by their interaction with carboxyl groups.[54] Then, three cycles of ZnS passivation coating using SILAR method were carried out. Sandwich-type cells were constructed by assembling QD-sensitized TiO_2 film electrode and Cu_2S/brass counter electrode, which were separated with hollowed Scotch spacer. Then polysulfide electrolyte was injected and inhaled to the layers by capillary effect. The *J–V* curves of the solar cells under the illumination of an AM 1.5G solar simulator with an intensity of 100 mW cm^{-2} (1 full sun) are shown in Fig. 4a, and the extracted photovoltaic parameters are collected in Table S1.† It is noted that for the photovoltaic performance measurement at least three cells were constructed. The trends of the photovoltaic parameters are shown in Fig. 5 as functions of zinc contents. FF about 51.1 (±3.9)% and V_{oc} about 0.526 (±0.04) V are not sensitive to zinc contents where as J_{sc} has a maximum of 22.1 (±3.5) mA cm^{-2} at ZCIS-5.0 due to the compromising between charge recombination and injection barrier effects. Correspondingly, a maximum PCE of 5.9 (±0.5)% was achieved at the doped $CuInS_2$ QDs of ZCIS-5.0. After the doping with zinc at optimized conditions, the average PCE of QDSCs under one full sun illumination is increased from 5.21% for pure QDs to 5.90% for doped QDs, a remarkable increase of 13.2%. As a comparison, J_{sc} and PCE of pure $CuInS_2$ QDSCs were measured to be 18.9 (±0.9) mA cm^{-2} and 5.21 (±0.3)%, respectively. Although the obtained efficiencies are lower than the values of 7.06% for glaring $CuInS_2$/ZnS QDSCs[23] and 11.6% for Zn–Cu–In–Se QDSCs,[10] the improvement of photovoltaic performance in doped $CuInS_2$ QDSCs is still encouraging, especially, taking the facile synthesis into consideration. The remarkable enhanced J_{sc} for QDSCs of ZCIS-5.0 (from 18.9 to 22.1 mA cm^{-2}) was thought introduced by increased efficient electron injection from both extended photoresponse range, which confirmed by red shifted absorption band edges in UV-vis absorption spectra (Fig. 1), and moderate lifetime PL with increased QY (Fig. 3a and S1†), while other QDSCs possessed either or neither of the two sources.

Table 2 Fitting parameters deriving from the equation *I*(*t*)

QD	τ_1/ns	τ_2/ns	α_1/%	α_2/%	F_1/%	F_2/%	τ_{ave}/ns
ZCIS-50	21.7	160.9	24.88	75.12	4.3	95.7	154.9
ZCIS-25	20.2	161.0	23.53	76.47	3.7	96.3	155.8
ZCIS-10	22.4	182.7	19.63	80.37	2.9	97.1	178.0
ZCIS-7.5	21.0	172.7	20.52	79.48	3.0	97.0	168.1
ZCIS-5.0	20.5	178.5	17.88	82.12	2.4	97.6	174.6
ZCIS-2.5	24.4	185.9	23.37	77.89	3.8	96.2	179.8
CIS	19.4	222.7	16.81	83.19	1.7	98.3	219.2

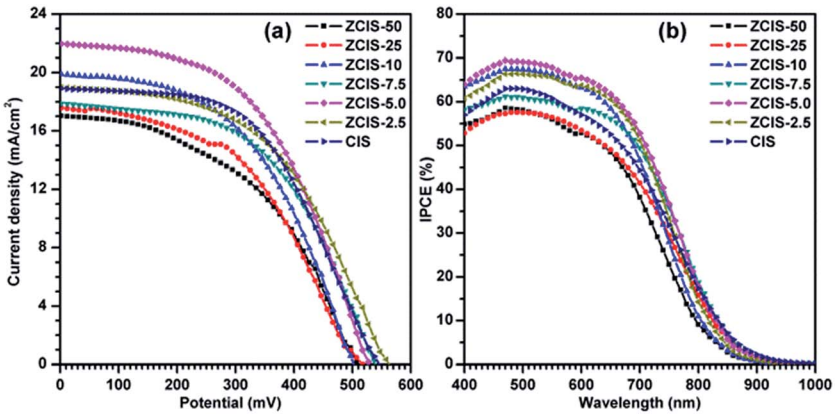

Fig. 4 Photovoltaic performances of doped $CuInS_2$ QDs sensitized QDSCs with different zinc contents. (a) Current–voltage characteristics, recorded under AM 1.5 radiation with an incident power of 100 mW cm^{-2}. (b) Incident photon conversion efficiency (IPCE) curves.

IPCE represents the percentage of incident photons that are converted to charge carriers and collected at the electrode surface. The IPCE spectra shown in Fig. 4b exhibit photoresponses roughly matching with the absorption spectra of QDs. The photoresponse ranges in the IPCE spectra are wider than the corresponding absorption ranges of doped $CuInS_2$ QDs, which can be ascribed to the light scattering effect by 200 nm TiO_2 particles in mesoporous TiO_2 layer. The IPCE spectrum of ZCIS-5.0 based QDSCs exhibits a strong photoresponse over 50% within the window below 750 nm and reaches the maximum value of 69% at 500 nm, while the other QDSCs show the weak photoresponse either in shorter wavelength window or low convert efficiency, consistent with the aforementioned J_{sc} trend (Fig. 4a). The J_{sc} values obtained by integrating IPCE spectra are 12.15, 13.14, 14.68, 14.49, 15.81, 15.07 and 14.10 mA cm^{-2}, respectively. They are generally smaller than the corresponding values by *J–V* characteristics. The systematic discrepancy can be may be explained by limited charge separation and collection efficiencies due to lower light intensities from monochromator in IPCE than that of AM 1.5G illumination in *J–V* characteristics.[21] Previously reported photoresponse range of CdSe and CdS/CdSe QDs sensitizers in QDSCs are typically less than 700 nm.[54–57] In the current work, the ranges are extended to near-infrared region (*ca.* 950 nm), which were realized by properly controlling band gap of doped $CuInS_2$, resulting in effective light harvesting utilization and reinforced photocurrents.

Electron injection rate from absorber to the conduction band of TiO_2 is an important parameter in QDSCs.[58] It has been demonstrated that the excited-state features of QDs depend on the substrate to which they are attached.[23,59] To evaluate the kinetics of charge transfer from QDs to TiO_2, PL decay

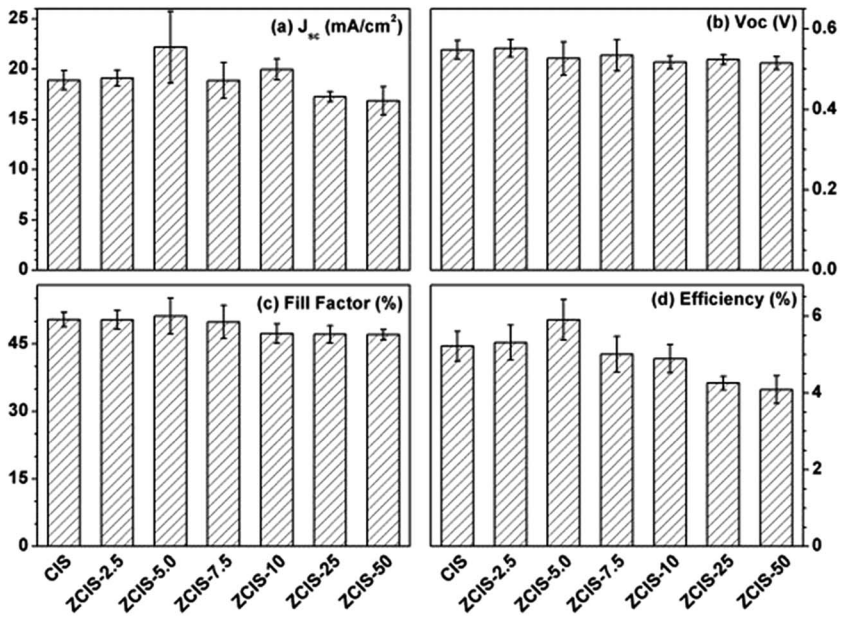

Fig. 5 The photovoltaic parameters of doped $CuInS_2$ based QDSCs with different zinc contents.

measurements were carried out for QDs deposited on both TiO_2 and insulating SiO_2 substrate.[60] An additional deactivation route was formed after doped $CuInS_2$ and pure $CuInS_2$ QDs deposited on TiO_2 mesoporous films, in which electrons could easily transfer to TiO_2 for their lower conduction band edge. As compared in Fig. 6, the recoveries of bleaching of doped $CuInS_2$ of ZCIS-5.0 and pure $CuInS_2$ QDs on insulating TiO_2 are relatively faster than those on SiO_2, which. These results confirm promoted electron injections from QDs to TiO_2.[60]

Biexponential decay model was used to fit the lifetime traces. The fitting results and calculated average lifetime (τ_{av}) are listed in Table 3. The rate constants of electron transfer from QD to TiO_2, k_{et}, can be estimated by comparing the PL decay processes of the QDs on TiO_2 to those on SiO_2, following eqn (1).

$$k_{et} = 1/\tau_{av(TiO_2)} - 1/\tau_{av(SiO_2)} \quad (1)$$

where $\tau_{av(TiO_2)}$ and $\tau_{av(SiO_2)}$ are the average lifetimes of QDs on TiO_2 and SiO_2 substrates, respectively. Using eqn (1) and τ_{av} values in Table 3 gives $k_{et} = 2.99 \times 10^{10}\ s^{-1}$ for doped $CuInS_2$ QDs (ZCIS-5.0) and $0.276 \times 10^{10}\ s^{-1}$ for pure $CuInS_2$ QDs, different by a magnitude order. The conduction band of doped $CuInS_2$ QDs provides the driving force of electron injection. The upper conduction band, originated from zinc doped in $CuInS_2$ QDs, results in an enhanced driving force, corresponding to a higher value of k_{et}, which explains the larger rate constant of electron transfer for ZCIS-5.0 QDs than that for pure $CuInS_2$ QDs. A similar correlation of the electron transfer rate with the conduction band energy of QDs was established by varying the particle size or composition.[7,61] Earlier studies with quantized CdSe and $CuInS_2$ have shown size dependent electron injection process dictated by the energy gap between the conduction band of CdSe or $CuInS_2$ and TiO_2 as well as acceptor density of states.[7,8] However, the dilemma will be encountered if the donor and acceptor sub-bandgap states from excess defects hold the energy level of conduction and valence bands. Other than intrinsic conduction band, the trap site (donor level) lying close to the conduction band of the QDs may dominate electron injection. According to successively decreased PL lifetimes and reduced share of their slow components, doped $CuInS_2$ QDs with high zinc contents may produce additional defects, which diminish the driving force for electron injection and lead to deteriorated performance of QDSCs.

Table 3 Fitting results of PL emission decay of doped and pure $CuInS_2$ QDs on TiO_2 and SiO_2 substrates

Sample	τ_1/ns	α_1/%	τ_2/ns	α_2/%	τ_{ave}/ns	k_{et} ($\times 10^{10}/s^{-1}$)
ZCIS-5.0@TiO_2	0.22	32.72	3.4	67.28	3.3	2.99
ZCIS-5.0@SiO_2	17.3	9.39	238.1	90.61	236.4	
CIS@TiO_2	3.55	80.68	41.4	19.32	31.4	0.276
CIS@SiO_2	23.05	9.92	240.12	90.08	237.8	

4. Conclusion

In this paper we report a facile synthesis of doped $CuInS_2$ QDs under air circumstance by the organometallic high temperature method. Owing to the modulation on doped zinc contents, features of tunable photoluminescence of doped $CuInS_2$ QDs with improved lifetime and QY have been demonstrated. It was shown that donor–acceptor pair recombination contributes to above 95% of the whole emission profiles. The optical and electronic properties of doped $CuInS_2$ QDs have significant effects on the performance of QDSCs. ZCIS-5.0 QDs based QDSCs exhibited PCE of 5.90% under one full sun illumination, higher than the value of 5.21% for pure $CuInS_2$ QDs. The improvement is mainly originated from broadened optoelectronic response range up to ~950 nm. IPCE values are over ~50% within the window below 750 nm and a maximum of 69% is obtained at 500 nm. Furthermore, faster electron injection of doped $CuInS_2$ from QDs to TiO_2 films, with k_{et} increased from $0.276 \times 10^{10}\ s^{-1}$ to $2.99 \times 10^{10}\ s^{-1}$, plays another important role in increasing PCE. The facile synthetic approach combined with composition modulation on dopant provides practical guidance to the future development of high performance QDSCs.

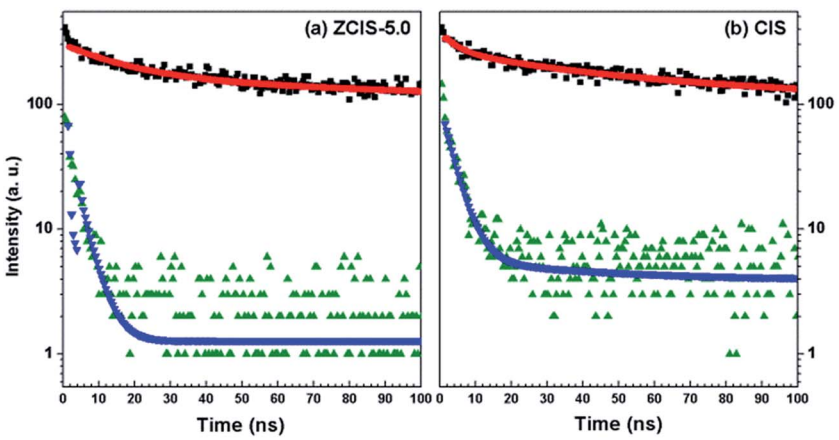

Fig. 6 PL emission decay plots of doped (a) and pure (b) $CuInS_2$ QDs on TiO_2 (olive for decay and blue for fit) and SiO_2 (black for decay and red for fit) films, respectively.

Acknowledgements

This work was financially supported by the funds from the National Natural Science Foundation of China (51572199, 51420105002, 51302194, 61471270) and the Key Lab of Novel Thin Film Solar Cells, Chinese Academy of Sciences (KF201603).

References

1 A. D. Yoffe, *Adv. Phys.*, 2001, **50**, 1–208.
2 O. E. Semonin, J. M. Luther, S. Choi, H.-Y. Chen, J. Gao, A. J. Nozik and M. C. Beard, *Science*, 2011, **334**, 1530–1533.
3 C.-H. M. Chuang, P. R. Brown, V. Bulović and M. G. Bawendi, *Nat. Mater.*, 2014, **13**, 796–801.
4 D. Bera, L. Qian, T.-K. Tseng and P. H. Holloway, *Materials*, 2010, **3**, 2260.
5 K. Chen, J. Zhou, W. Chen, Q. Chen, P. Zhou and Y. Liu, *Nanoscale*, 2016, **8**, 5146–5152.
6 K. Chen, J. Zhou, W. Chen, P. Zhou, F. He and Y. Liu, *Part. Part. Syst. Charact.*, 2015, **32**, 999–1005.
7 I. Robel, M. Kuno and P. V. Kamat, *J. Am. Chem. Soc.*, 2007, **129**, 4136–4137.
8 D. H. Jara, S. J. Yoon, K. G. Stamplecoskie and P. V. Kamat, *Chem. Mater.*, 2014, **26**, 7221–7228.
9 Z. Du, Z. Pan, F. Fabregat-Santiago, K. Zhao, D. Long, H. Zhang, Y. Zhao, X. Zhong, J.-S. Yu and J. Bisquert, *J. Phys. Chem. Lett.*, 2016, **7**, 3103–3111.
10 J. Du, Z. L. Du, J. S. Hu, Z. X. Pan, Q. Shen, J. K. Sung, D. H. Long, H. Dong, L. T. Sun, X. H. Zhong and L. J. Wan, *J. Am. Chem. Soc.*, 2016, **138**, 4201–4209.
11 P. V. Kamat, *J. Phys. Chem. Lett.*, 2013, **4**, 908–918.
12 F. Liu, J. Zhu, J. F. Wei, Y. Li, L. H. Hu and S. Y. Dai, *Prog. Chem.*, 2013, **25**, 409–418.
13 H. Y. Wei, G. S. Wang, H. J. Wu, Y. H. Luo, D. M. Li and Q. B. Meng, *Acta Phys.-Chim. Sin.*, 2016, **32**, 201–213.
14 H. K. Jun, M. A. Careem and A. K. Arof, *Renewable Sustainable Energy Rev.*, 2013, **22**, 148–167.
15 H. Zhong, Z. Bai and B. Zou, *J. Phys. Chem. Lett.*, 2012, **3**, 3167–3175.
16 S. R. Kodigala, in *Thin Films and Nanostructures*, ed. K. Subba Ramaiah, Academic Press, 2010, vol. 35, pp. 319–391.
17 R. G. Xie, M. Rutherford and X. G. Peng, *J. Am. Chem. Soc.*, 2009, **131**, 5691–5697.
18 H. McDaniel, N. Fuke, J. M. Pietryga and V. I. Klimov, *J. Phys. Chem. Lett.*, 2013, **4**, 355–361.
19 Y. Liu, T. Chen, Z. Peng, L. Wu, K. Chen, P. Zhou, L. Wang and W. Chen, *J. Alloys Compd.*, 2016, **658**, 76–84.
20 P. K. Santra, P. V. Nair, K. George Thomas and P. V. Kamat, *J. Phys. Chem. Lett.*, 2013, **4**, 722–729.
21 T.-L. Li, Y.-L. Lee and H. Teng, *Energy Environ. Sci.*, 2012, **5**, 5315–5324.
22 Z. Peng, Y. Liu, W. Chen, K. Chen, J. Chen and J. Chen, *J. Alloys Compd.*, 2017, **701**, 131–137.
23 Z. X. Pan, I. Mora-Sero, Q. Shen, H. Zhang, Y. Li, K. Zhao, J. Wang, X. H. Zhong and J. Bisquert, *J. Am. Chem. Soc.*, 2014, **136**, 9203–9210.
24 J.-Y. Kim, J. Yang, J. H. Yu, W. Baek, C.-H. Lee, H. J. Son, T. Hyeon and M. J. Ko, *ACS Nano*, 2015, **9**, 11286–11295.
25 M. C. Hanna and A. J. Nozik, *J. Appl. Phys.*, 2006, **100**, 074510.
26 Z. Yang, C.-Y. Chen, P. Roy and H.-T. Chang, *Chem. Commun.*, 2011, **47**, 9561–9571.
27 S. Rühle, M. Shalom and A. Zaban, *ChemPhysChem*, 2010, **11**, 2290–2304.
28 L. Li, A. Pandey, D. J. Werder, B. P. Khanal, J. M. Pietryga and V. I. Klimov, *J. Am. Chem. Soc.*, 2011, **133**, 1176–1179.
29 J. W. Yang, J. Wang, K. Zhao, T. Izuishi, Y. Li, Q. Shen and X. H. Zhong, *J. Phys. Chem. C*, 2015, **119**, 28800–28808.
30 A. M. Smith and S. Nie, *Acc. Chem. Res.*, 2010, **43**, 190–200.
31 Y. C. Cao, *Science*, 2011, **332**, 48–49.
32 D. V. Talapin, J.-S. Lee, M. V. Kovalenko and E. V. Shevchenko, *Chem. Rev.*, 2010, **110**, 389–458.
33 T. Omata, K. Nose, K. Kurimoto and M. Kita, *J. Mater. Chem. C*, 2014, **2**, 6867–6872.
34 D. H. Jara, K. G. Stamplecoskie and P. V. Kamat, *J. Phys. Chem. Lett.*, 2016, **7**, 1452–1459.
35 B. K. Chen, H. Z. Zhong, W. Q. Zhang, Z. A. Tan, Y. F. Li, C. R. Yu, T. Y. Zhai, Y. S. Bando, S. Y. Yang and B. S. Zou, *Adv. Funct. Mater.*, 2012, **22**, 2081–2088.
36 Y. K. Kim, S. H. Ahn, K. Chung, Y. S. Cho and C. J. Choi, *J. Mater. Chem.*, 2012, **22**, 1516–1520.
37 W. Y. Liu, Y. Zhang, J. Zhao, Y. Feng, D. Wang, T. Q. Zhang, W. Z. Gao, H. R. Chu, J. Z. Yin, Y. D. Wang, J. Zhao and W. W. Yu, *J. Lumin.*, 2015, **162**, 191–196.
38 W. Peng, J. Du, Z. Pan, N. Nakazawa, J. Sun, Z. Du, G. Shen, J. Yu, J.-S. Hu, Q. Shen and X. Zhong, *ACS Appl. Mater. Interfaces*, 2017, **9**, 5328–5336.
39 G. Halder and S. Bhattacharyya, *J. Mater. Chem. A*, 2017, **5**, 11746–11755.
40 D. C. Pan, L. J. An, Z. M. Sun, W. Hou, Y. Yang, Z. Z. Yang and Y. F. Lu, *J. Am. Chem. Soc.*, 2008, **130**, 5620–5621.
41 M. Grabolle, M. Spieles, V. Lesnyak, N. Gaponik, A. Eychmuller and U. Resch-Genger, *Anal. Chem.*, 2009, **81**, 6285–6294.
42 H. Zhong, Z. Wang, E. Bovero, Z. Lu, F. C. J. M. van Veggel and G. D. Scholes, *J. Phys. Chem. C*, 2011, **115**, 12396–12402.
43 J. Zhang, R. Xie and W. Yang, *Chem. Mater.*, 2011, **23**, 3357–3361.
44 D. Deng, Y. Chen, J. Cao, J. Tian, Z. Qian, S. Achilefu and Y. Gu, *Chem. Mater.*, 2012, **24**, 3029–3037.
45 W. Zhang and X. Zhong, *Inorg. Chem.*, 2011, **50**, 4065–4072.
46 C.-C. Chang, J.-K. Chen, C.-P. Chen, C.-H. Yang and J.-Y. Chang, *ACS Appl. Mater. Interfaces*, 2013, **5**, 11296–11306.
47 *Principles of Fluorescence Spectroscopy*, ed. J. R. Lakowicz, Springer, US, Boston, MA, 2006, pp. 97–155, DOI: 10.1007/978-0-387-46312-4_4.
48 V. K. Komarala, C. Xie, Y. Wang, J. Xu and M. Xiao, *J. Appl. Phys.*, 2012, **111**, 124314.
49 S. L. Castro, S. G. Bailey, R. P. Raffaelle, K. K. Banger and A. F. Hepp, *J. Phys. Chem. B*, 2004, **108**, 12429–12435.
50 S. B. Zhang, S.-H. Wei, A. Zunger and H. Katayama-Yoshida, *Phys. Rev. B: Condens. Matter Mater. Phys.*, 1998, **57**, 9642–9656.
51 C. Rincón and R. Márquez, *J. Phys. Chem. Solids*, 1999, **60**, 1865–1873.

52 B. J. Stanbery, *Crit. Rev. Solid State Mater. Sci.*, 2002, **27**, 73–117.
53 B.-K. Pong, B. L. Trout and J.-Y. Lee, *Langmuir*, 2008, **24**, 5270–5276.
54 H. Zhang, K. Cheng, Y. M. Hou, Z. Fang, Z. X. Pan, W. J. Wu, J. L. Hua and X. H. Zhong, *Chem. Commun.*, 2012, **48**, 11235–11237.
55 Z. Pan, H. Zhang, K. Cheng, Y. Hou, J. Hua and X. Zhong, *ACS Nano*, 2012, **6**, 3982–3991.
56 F. Liu, J. Zhu, J. Wei, Y. Li, L. Hu, Y. Huang, O. Takuya, Q. Shen, T. Toyoda, B. Zhang, J. Yao and S. Dai, *J. Phys. Chem. C*, 2014, **118**, 214–222.
57 F. Huang, L. Zhang, Q. Zhang, J. Hou, H. Wang, H. Wang, S. Peng, J. Liu and G. Cao, *ACS Appl. Mater. Interfaces*, 2016, **8**, 34482–34489.
58 K. Tvrdy, P. A. Frantsuzov and P. V. Kamat, *Proc. Natl. Acad. Sci. U. S. A.*, 2011, **108**, 29–34.
59 G. Wang, H. Wei, Y. Luo, H. Wu, D. Li, X. Zhong and Q. Meng, *J. Power Sources*, 2016, **302**, 266–273.
60 J. Wang, I. Mora-Sero, Z. X. Pan, K. Zhao, H. Zhang, Y. Y. Feng, G. Yang, X. H. Zhong and J. Bisquert, *J. Am. Chem. Soc.*, 2013, **135**, 15913–15922.
61 I. Robel, V. Subramanian, M. Kuno and P. V. Kamat, *J. Am. Chem. Soc.*, 2006, **128**, 2385–2393.